

OPTIMIZING THE ENERGY PERFORMANCE OF A HYBRID PVT AIR COLLECTOR WITH PARABOLIC TROUGH CONCENTRATOR AND HELIOSTAT

PASERA Joanès Keneddy¹, HARITHI BEN Daoud Ben Attoumane¹, DONA Victorien Bruno²

¹PhD student, Laboratory of Applied Physics and Renewable Energies (LPADER), Ecole Doctoral Génie du Vivant et Modélisation (EDGVM), University of Mahajanga, Madagascar

²Professor, Laboratory of Applied Physics and Renewable Energies (LPADER), Ecole Doctoral Génie du Vivant et Modélisation (EDGVM), University of Mahajanga, Madagascar

ABSTRACT

The work proposed in this paper consists of a combination of three solar energy conversion technologies (Air PVT - Cylindro-Parabolic Concentrator - Heliostat) for the continuous production of electrical and thermal energy. To enhance system performance, the Photovoltaic Thermal Air Collector is placed in the focal zone of a Concentric Cylindro-Parabolic Thermal Collector and the Heliostat sun-tracking system (PVT-CCPH). The maximum power output of the PVT hybrid air collector is controlled by a Maximum Power Point Tracking (MPPT) control system. This system (PVT-CCPH) is designed to supply a resistive load. In order to maintain the characteristics of the electrical load with those of the PVT at the MPP maximum power point, a DC-DC converter has been used. The system's autonomy will be ensured by a storage system. This combination offers an interesting alternative to ordinary photovoltaic modules and conventional thermal collectors installed separately. The aim of this study is to improve the energy performance of the PVT-CCPH hybrid system adapted to the climate in the city of Mahajanga. The work therefore focused on modeling and simulating this hybrid system using Matlab and simulink software. In this study, mathematical models were developed for each component of the system in order to obtain the expected results.

Keyword : - Solar irradiation, Air PVT, Fins, Cylindro-Parabolic, Heliostat, MPPT, Perturbe & Observe (P&O), Inverter, Performance

1. INTRODUCTION

Madagascar offers highly favorable conditions for the implementation of promising solar energy projects. In fact, the country enjoys one of the highest levels of solar irradiation [1]. Numerous technologies are being used to harness this solar radiation, including conventional photovoltaic (PV) and concentrated photovoltaic (CPV) solar power plants [2,3]. But CPV installations remain limited compared to other technologies, with only small-scale CPV plants installed in the country for research and demonstration purposes. The main objective of this study is to maximize the electrical power and hot air recovery released from the hybrid Photovoltaic Thermal Air Collector equipped with a Cylindro-Parabolic Concentrator and Heliostat (PVT-CCPH). The most encouraging advantage of systems equipped with Cylindro-Parabolic Concentrators and Heliostats is the ability to collect a significant amount of solar radiation thanks to stationary operation and without the need for a tracking system. However, the integration of a Cylindro-Parabolic Concentrator leads to an increase in the temperature of the PV cells, which has a considerable impact on their electrical efficiency. To cool the PV modules, aluminum alloy cooling fins are added to the rectangular cooling channel. The extracted hot air could be used to dry products. The work focused on modeling and simulating this hybrid system

using Matlab and simulink software. Mathematical models were developed for each component of the system, in order to obtain the expected results.

2. METHODOLOGIES

2.1.1 System configuration

The PVT hybrid air collector consists of several different layers : glass, PV cells, EVA encapsulation film, tedlar, upper absorber with fins, heat transfer air, lower absorber, thermal insulation.

This PVT is placed between two reflector systems : the first reflector is a heliostat. It first collects and reflects solar radiation towards the parabolic trough. Its main role is to direct the sun's rays ; whatever the sun's position in the sky or even on the horizon, solar radiation is always efficiently concentrated towards the parabolic trough concentrator [3,4,5]. The second reflector is the parabolic trough, whose main role is to focus solar energy onto a focal line where the PVT collector is located [3,6].

MPPT control continuously adapts the electrical load connected to the energy source to maximize efficiency and the amount of energy produced, despite variations in solar irradiation and temperature [7]. The boost converter (DC-DC) is capable of adjusting the average value of the output voltage by setting the value of the duty cycle [3]. The battery stores energy to power the inverter. It enables energy to be supplied even when the main source such as PVT is absent or insufficient. The voltage inverter (DC-AC) transforms a direct current source from the battery into an alternating voltage to supply AC loads.

The figure below shows the complete system configuration of a hybrid concentrating solar collector.

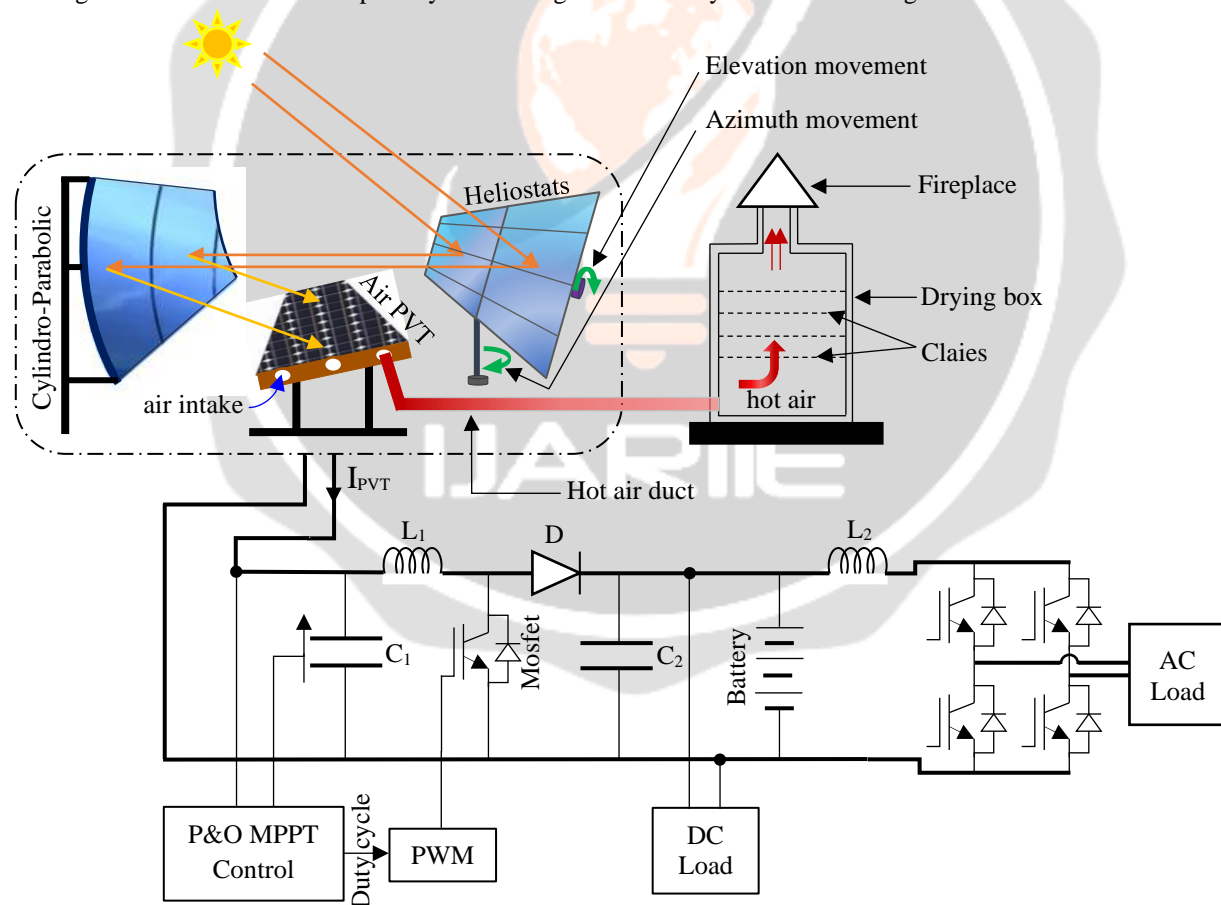


Fig-1: System configuration PVT-CCP-H

2.1.2 Mathematical modeling

A cross-section of a PVT hybrid air collector is shown in Figure 2 [8,9,10].

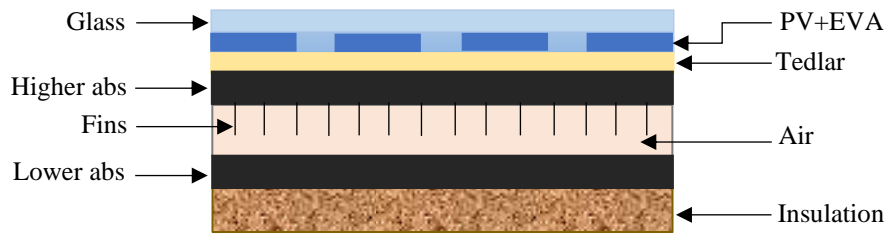


Fig-2 : Cross-section of PVT hybrid air collector.

Figure 3 shows the equivalent electrical circuit of the PVT hybrid air collector.

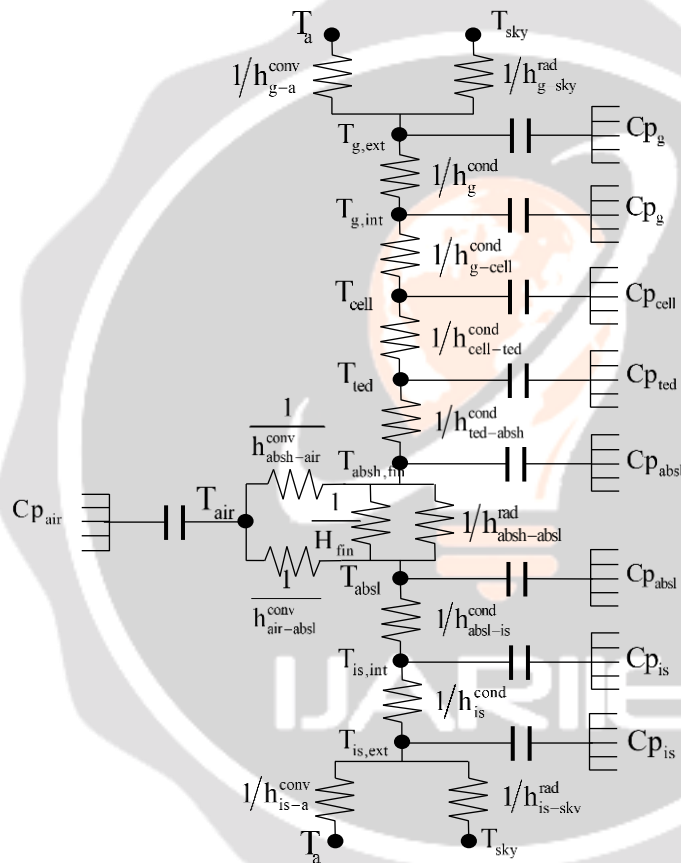


Fig-3 : Equivalent electrical circuit of the PVT hybrid air collector [11,12].

2.1.3 Study hypothesis

Before modeling, it is necessary to specify certain calculation assumptions [3,8,9,10,13,14] :

- The sky can be assimilated to a black body with an equivalent temperature calculated ;
- Heat transfer is considered to be one-dimensional through the layers of the system.
- The ambient temperature is the same around the sensor ;
- Ground temperature is taken to be equal to ambient temperature
- EVA's transmission coefficient is 100%.
- The mass flow rate is uniform in the air layer duct ;

- The wind speed on the face of the collector is assumed to be constant ;
- The thermo-physical properties of the fluid are a function of temperature ;
- The absorber's thermal and geometric properties are equal ;
- The thermal properties of the fin are equal to those of the absorber ;
- The effect of shading and dust on the collector is negligible.
- Heliostat concentration is equal to one.
- The resistive load is connected after the filter capacitor C_2 , at the Boost output. All other components located after the C_2 such as (battery, inductor, voltage inverter, etc.) are temporarily ignored (neglected) in this study. The load is therefore modeled solely by a resistor.

2.1.4 Equating the system

The following equations were obtained by applying Ohm's law to the mesh node from the equivalent circuit shown in figure 3 [8,9,10,11,14,15] :

Node 1 : outer face of glass

$$\frac{m_g C_p g}{S_g} \left(\frac{dT_{g,ext}}{dt} \right) = G_i \cdot C - h_{g-a}^{conv} (T_{g,ext} - T_a) - h_g^{cond} (T_{g,ext} - T_{g,int}) - h_{g-sky}^{rad} (T_{g,ext} - T_{sky}) \quad (01)$$

Node 2 : inner face of glass pane

$$\frac{m_g C_p g}{S_g} \left(\frac{dT_{g,int}}{dt} \right) = \alpha_g \cdot G_i \cdot C + h_g^{cond} (T_{g,ext} - T_{g,int}) - h_{g-cell}^{cond} (T_{g,int} - T_{cell}) \quad (02)$$

Node 3 : PV cell

$$\frac{m_{cell} C_p cell}{S_{cell}} \left(\frac{dT_{cell}}{dt} \right) = \tau_g \cdot \alpha_{cell} G_i \cdot C + h_{g-cell}^{cond} (T_{g,int} - T_{cell}) - h_{cell-ted}^{cond} (T_{cell} - T_{ted}) - \frac{Q_{elec}}{S_{cell}} \quad (03)$$

Node 4 : tedlar layer

$$\frac{m_{ted} C_p ted}{S_{ted}} \left(\frac{dT_{ted}}{dt} \right) = h_{cell-ted}^{cond} (T_{cell} - T_{ted}) - h_{ted-absh}^{cond} (T_{ted} - T_{absh}) \quad (04)$$

Node 5 : top absorber layer and fins

$$\frac{m_{abs} C_p abs}{S_{abs}} \left(\frac{dT_{absh}}{dt} \right) = h_{cell-absh}^{cond} (T_{ted} - T_{absh}) - h_{absh-air}^{conv} (T_{absh} - T_{air}) - H_{fin} (T_{absh} - T_{air}) - h_{absh-absl}^{rad} (T_{absh}^4 - T_{absl}^4) \quad (05)$$

$$\text{With [8,16] : } H_{fins} = h_{absh-air}^{conv} \cdot \eta_{fins} \quad (06)$$

$$\text{Where : } \eta_{fins} = 1 - \frac{N \cdot S_{fins}}{S_t} (1 - \eta_b), \text{ and } \eta_b = \frac{\tanh \left(H \cdot \sqrt{\frac{2Lh_f}{\lambda_{fins} e_{fins}}} \right)}{H \cdot \sqrt{\frac{2Lh_f}{\lambda_{fins} e_{fins}}}} \quad (07)$$

Node 6 : air layer

$$\frac{m_{air} C_p air}{S_{air}} \left(\frac{dT_f}{dt} \right) = h_{absh-air}^{conv} (T_{absh} - T_{air}) + H_{fin} (T_{absh} - T_{air}) + h_{air-absl}^{conv} (T_{absl} - T_{air}) - \dot{m} C_p_{air} (T_{air,out} - T_{air,in}) \quad (08)$$

Node 7 : lower absorber layer

$$\frac{m_{absl} C_p absl}{S_{abB}} \left(\frac{dT_{absl}}{dt} \right) = h_{air-absl}^{conv} (T_{air} - T_{absl}) - h_{absl-is}^{cond} (T_{absl} - T_{is,int}) + h_{absh-absl}^{rad} (T_{absh}^4 - T_{absl}^4) \quad (09)$$

Node 8 : inside face of insulation

$$\frac{m_{is} C_{p_{is}}}{S_{is}} \left(\frac{dT_{is,int}}{dt} \right) = h_{absl-is}^{cond} (T_{absl} - T_{is,int}) - h_{is}^{cond} (T_{is,int} - T_{is,ext}) \quad (10)$$

Node 9 : outer face of insulation

$$\frac{m_{is} C_{p_{is}}}{S_{is}} \left(\frac{dT_{is,ext}}{dt} \right) = h_{is}^{cond} (T_{is,int} - T_{is,ext}) - h_{is-a}^{conv} (T_{is,ext} - T_a) - h_{is-sol}^{rad} (T_{is,ext} - T_{sol}) \quad (11)$$

2.1.5 Heat exchange coefficients

❖ Conductive heat transfer coefficient

In general, the conductive heat transfer coefficient between two layers of adjacent components m_i and n_i is given by the empirical relationship as follows [9] :

$$h_{m_i-n_i}^{cond} = \left(\frac{e_{m_i}}{\lambda_{m_i}} + \frac{e_{n_i}}{\lambda_{n_i}} \right)^{-1} \quad (12)$$

❖ Convective heat transfer coefficients [8,9].

The Mac Adams correlation was used to determine the heat exchange between the glass and the environment:

$$h_{v-a}^{conv} = 5,6 + 3,8V_{vent} \quad \text{where } V_{vent} \text{ is the wind speed} \quad (13)$$

Convective heat exchange coefficients are calculated using empirical correlations based on the Nusselt number:

$$h_{air}^{conv} = \frac{N_u \lambda_{air}}{D_h} \quad (14)$$

Heat transfer between absorber and fluid :

$$h_{abs-air}^{conv} = \left(\frac{e_{abs}}{\lambda_{abs}} + \frac{1}{h_{air}^{conv}} \right)^{-1} \quad (15)$$

In our case, the Nusselt number is calculated according to the flow regime, which is expressed by the following equations [17,18] :

- For laminar flow ($Re_{air} < 2300$)

$$Nu = N_{\infty} + \frac{a [Pr_{air} \cdot Re_{air} \cdot D_h / L]^{m'}}{1 + b [Pr_{air} \cdot Re_{air} \cdot D_h / L]^{n'}} \quad (\text{Heaton's empirical correlation}) \quad (16)$$

With : $a = 0.00190$, $b = 0.00563$, $N_{\infty} = 5.4$, $Pr = 0.7$, $n' = 1.17$, $m' = 1.71$

- For transient flow ($2300 < Re_{air} < 6000$)

$$Nu = 0.0214 \times (Re_{air}^{0.8} - 100) \times Pr_{air}^{0.4} \times \left[1 + (D_h / L)^{0.66} \right] \quad (17)$$

With conditions : $0.5 \leq Pr_{air} \leq 1.5$ $2300 < Re_{air} < 10^6$ and $0 < D_h / L < 1$

- For turbulent flow ($Re_{air} > 6000$)

$$Nu = 0.023 \times (Re_{air})^{0.8} \times (Pr_{air})^{0.4} \quad (\text{the empirical correlation of Tan and Charters (1970)}) \quad (18)$$

With : $0.6 \leq Pr_{air} \leq 160$ $Re_{air} \geq 10000$ and $L / D_h \geq 10$

The Prandtl and Reynolds number is defined by the following relationship [9] :

$$Pr_{air} = \frac{\mu_{air} \cdot Cp_{air}}{\nu_{air}} \text{ and } Re_{air} = \frac{V_{air} D_h}{\nu_{air}}, \text{ with } D_h = \frac{4(1 \times H_c)}{2(1 + H_c)} \tag{19}$$

Where : D_h , ℓ and H_c are hydraulic pipe diameter, sensor width and air pipe height respectively.

❖ **Coefficient of radiant heat exchange** [8,9,10].

The radiative exchange coefficient is calculated using empirical formulas as follows:

$$h_{g-sky}^{rad} = \epsilon_g \cdot \sigma \cdot (T_{g,ext} + T_{sky}) (T_{g,ext}^2 + T_{sky}^2) \tag{20}$$

$$h_{absh-absl}^{rad} = \sigma \frac{(T_{absh} + T_{absl}) (T_{absh}^2 + T_{absl}^2)}{\left(\frac{1}{\epsilon_{absh}}\right) + \left(\frac{1}{\epsilon_{absl}}\right) - 1} \tag{21}$$

Where : $\sigma = 5,67 \times 10^{-8}$, Stephan Boltzmann's constant ;

$T_{sky} = 0,0552 \cdot (T_a)^{1,5}$ The temperature of the sky is given by the Swinbank relation.

With : $T_a = \left[\frac{T_{a,max} - T_{a,min}}{2} \right] \cdot \cos \left[\frac{(TSV - 12) \cdot \pi}{12} \right] + \left[\frac{T_{a,max} + T_{a,min}}{2} \right]$ ambient temperature.

The physical properties of air are assumed to vary linearly with temperature. Specific expressions have been given by Ebrahim and Alfege [10] :

- Specific gravity : $\rho_{air} = 1.1774 - 0.000359 \times T_{air}$;
- Specific heat : $Cp_{air} = [1.0057 + 0.000066 \times T_{air}] \times 1009$
- Thermal conductivity : $\lambda_{air} = 0.02624 + 0.0000758 \times T_{air}$;
- Dynamic viscosity : $\mu_{air} = [1.983 + 0.00184 \times T_{air}] \times 10^{-5}$

2.2 Concentric Cyllindro-Parabolic (CCP) solar collector

Another factor that is crucial to the smooth operation of a CCP system is the uniformity of irradiance at the concentrator outlet. Energy concentration is defined as the ratio of the average solar irradiance received on the surface of the PVT absorber (G_r) to the direct solar irradiance received at the CCP reflector aperture (G_o). The geometric concentration ratio is defined as the ratio between the CCP collector opening surface and the receiver surface (focused surface) [6,19].

$$C_e = \frac{G_r}{G_o} = C \times \rho_{ccp} \times \cos(\theta_{inc}) \text{ and } C = \frac{A_o}{A_r} = \frac{W_o}{W_r \times \cos(\theta_{inc})} = \frac{4 \times f \times \tan(\theta_o/2)}{W_r \times \cos(\theta_{inc})} \tag{22}$$

Where : ρ_{ccp} , θ_{inc} , θ_o , W_o and f represent collector reflectivity, concentrator aperture width, angle of incidence, aperture angle, focal length.

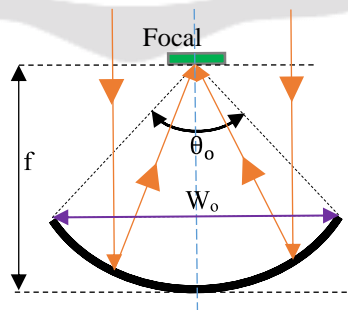


Fig-4 : Cross-section of a CCP [4].

2.3 PVT electrical model

The electrical behavior of the PVT system is strongly influenced by the intensity of solar irradiation and the temperature of the photovoltaic cells. For a single-diode model, the expression for the electric current leaving the photovoltaic collector is written as follows [7,12] :

$$I_{PV} = N_p \cdot I_{ph} - N_p \cdot I_0 \left[\exp \left(q \frac{V_{PV} + I_{PV} \cdot R_s}{n \cdot N_s \cdot K \cdot T} \right) - 1 \right] - \frac{V_{PV} + I_{PV} \cdot R_s}{R_{sh}} \quad (23)$$

Where : I_{ph} , I_0 , R_s , R_{sh} , q , N_s , N_p , n and K are respectively photon current, diode saturation current, series resistance, parallel resistance, electron charge, number of cells in series, number of cells in parallel, ideality factor, Boltzmann constant.

Current and voltage values vary with solar irradiation intensity and cell temperature, as shown in the following equations [12,20] :

$$\text{– Output current variation : } I(G_i C, T_{pv}) = I_{ref} + \Delta I = I_{ref} + k_i \left(\frac{G_i C}{G_{ref}} \right) \Delta T + \left(\frac{G_i C}{G_{ref}} - 1 \right) I_{sc,ref} \quad (24)$$

$$\text{– Output voltage variation : } V(G_i C, T_{pv}) = V_{ref} + \Delta V = V_{ref} + k_v \cdot \Delta T - R_s \cdot \Delta I \quad (25)$$

$$\text{– Short-circuit current variation : } I_{sc}(G_i C_e, T_{pv}) = \left(\frac{G_i C_e}{G_{ref}} \right) \times (k_i \cdot \Delta T + I_{sc,ref}) \quad (26)$$

$$\text{– Short-circuit current variation : } V_{oc}(G_i C, T_{pv}) = V_{oc,ref} + k_v \cdot \Delta T + n \cdot \ln \left(\frac{G_i C}{G_{ref}} \right) \quad (27)$$

$$\text{With : } \Delta T = T_{pv} - T_{pv,ref} \quad (28)$$

Where k_i and k_v are respectively the coefficient of variation of current and voltage as a function of temperature.

2.4 PVT hybrid air collector performance

The electrical power produced by the PVT hybrid solar collector is given by the following equation [9,14] :

$$Q_{elec} = \tau_g \cdot G_i \cdot C \cdot S_{cell} \cdot \eta_{ref} \cdot \exp[\beta(T_{cell} - T_{ref})] \quad (29)$$

Where : G_i is global solar irradiance.

The electrical efficiency of a PVT hybrid collector is the ratio of the electrical power produced to the power absorbed [8,9,18].

$$\eta_{elec} = \frac{Q_{elec}}{S_{cell} \cdot G_i \cdot C} \quad (30)$$

The overall PVT efficiency is the sum of the thermal efficiency and the thermal efficiency equivalent to the electrical efficiency [9,18].

$$\eta_{PVT} = \eta_{the} + \eta_{elec,the} \quad (31)$$

With : $\eta_{elec,the} = \frac{\eta_{elec}}{C_f}$ where C_f is the thermal energy conversion factor between 0.35 and 0.4.

3. RESULTS AND DISCUSSION

The Mahajanga study area is located in the north-western region of Madagascar with coordinates: 15°43' Sud (latitude), 46°19' Est (longitude). The ASECNA Mahajanga meteorological database was processed over a 14-year period (2010 to 2023), using the Page model to estimate global irradiance [21,22,23].

The photovoltaic collector used is made of polycrystalline silicon, with the parameters shown in Table 1. Characteristics are measured according to international specifications at a sunshine level of 1000 W.m⁻², a spectrum of AM 1.5 and a temperature of 25°C.

Table-1 : Electrical characteristics of a KC200GT photovoltaic module [7].

Experimental peak power P _{max}	200 W
Voltage at point of maximum power V _{pm}	26.3 V
Current at point of maximum power I _{pm}	7.61 A
Open circuit voltage V _{oc}	32.9 V
Short-circuit current I _{sc}	8.21 A
Voltage temperature coefficient k _v	-0.123 V/°C
Current temperature coefficient k _i	0.00318 A/°C
Operating temperature	-40 °C to +85 °C
Number of cells in series N _s	54
Number of parallel cells N _p	1
Reference yield	15 %
Dimension (L×l×h)	1425 mm × 990 mm × 36 mm

The characteristics of the various sensor components are shown in Table 2.

Table-2 : Features of PVT hybrid module components [10].

Features	Components		
	Glass coating	PV cell	Layer of tedlar
Density	2200 kg.m ⁻³	2330 kg.m ⁻³	1390 kg.m ⁻³
Specific heat	670 J.kg K ⁻¹⁻¹	836 J.kg K ⁻¹⁻¹	1400 J.kg K ⁻¹⁻¹
Thermal conductivity	0.93 W. K ⁻¹ .m ⁻¹	148 W. K ⁻¹ .m ⁻¹	0.033 W. K ⁻¹
Glazing emissivity	0.88	0.93	.m ⁻¹
Thickness	0.004 m	0.0003 m	0.88
Absorption coefficient	0.066	0.85	0.0005 m 0.5
Features	Absorber	Insulation	
Density	8000 kg.m ⁻³	2200 kg.m ⁻³	
Specific heat	36 J.kg K ⁻¹⁻¹	670 J.kg K ⁻¹⁻¹	
Thermal conductivity	410 W. K ⁻¹ .m ⁻¹	0.93 W. K ⁻¹	
Glazing emissivity	0.04	.m ⁻¹	
Thickness	0.0005 m	0.88	
Absorption coefficient	0.75	0.004 m 0.066	

Table 3 shows the boost converter component parameters.

Table-3 : Boost converter component parameters [3].

Parameters	Inductance	Capabilities C /C _{1 2}	Resistance
Values	290 μH	250 μF / 330 μF	35 Ω

3.1 Variation in solar irradiation and ambient temperature at Mahajanga

Figure 5 shows the simulated evolution of monthly average hourly irradiance and ambient temperature as a function of the typical day of the month in question, over the last 14 years. In Mahajanga, the highest hourly irradiance reached 940 W.m^{-2} around noon (in October), while the lowest value was 656 W.m^{-2} in January, due to the sun's angle of incidence. The figure also shows that ambient temperature varies throughout the day, depending on the month. Around midday, the ambient temperature reaches 33.12°C in April and drops to 30.81°C in February.

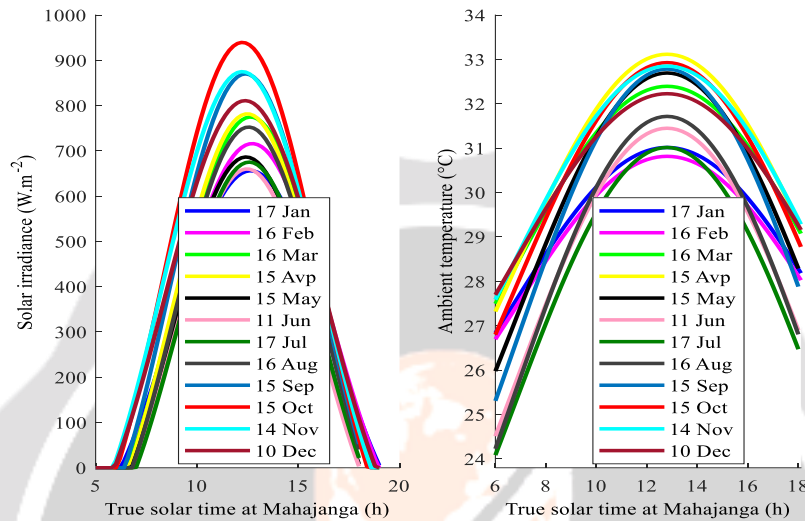


Fig-5 : Temporal variation in solar irradiance and ambient temperature.

3.2 Simulation of a parabolic trough concentrator

A parabolic trough is a linear translation of a two-dimensional parabolic reflector, with the focal point being a focal line. When the parabolic reflector is oriented parallel to the sun's rays, all incoming rays are redirected towards the focal line. The parabolic trough must follow the sun's movement precisely to keep the parabolic axis parallel to the sun's incident rays. Figure 6 shows that the aperture width, aperture angle and geometric concentration ratio of a cylinder vary with focal length. As the aperture angle increases, so does the focal length, enabling more of the sun's irradiance to be captured [6]. In our study, the width of the receiver is equal to that of the PVT ($l_{PVT} = 0.99 \text{ m}$). As a result, the pattern of concentration ratio and aperture width as a function of focal length is almost identical. For the concentration ratio $C = 2$, the aperture angle is of the order of 23.6° and the focal length is 2.36 m .

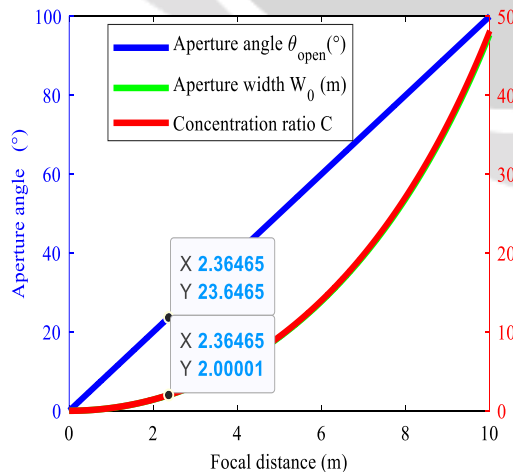


Fig-6 : Aperture width, aperture angle and concentration ratio as a function of focal length

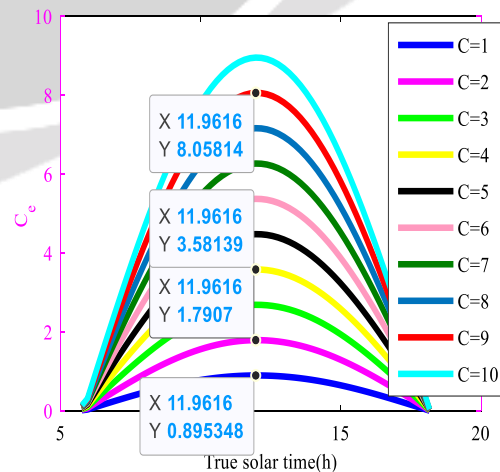


Fig-7 : Energy concentration

Figure 7 above shows the temporal evolution of energy concentration, which varies as a function of the geometric concentration ratio, the angle of incidence of solar rays and the optical properties of materials, such as reflectivity. This figure shows that energy concentration (C_e) follows the course of solar irradiation over the course of the day. As solar irradiance increases, so does energy concentration. We can also see that with a high geometric concentration ratio, the energy concentration value is high. For $C = 2$, energy concentration is 1.79 around midday. These results make it possible to estimate the actual intensity of energy available and used on the PVT sensor. Using the heliostat at the same time forces the CCP to achieve maximum optical efficiency, as the solar radiation coming from the heliostat is constantly perpendicular to the collector surface, making the angle of incidence of the rays equal to 0° . In this way, the CCP remains active and free from shading effects.

3.3 PVT hybrid collector element temperature

Figure 8 shows the temperature distribution of the PVT hybrid air collector as a function of time. For the month of October at the Mahajanga site, the temperatures of the PVT layers increase simultaneously with the increase in solar irradiation during the day, reaching their maximum value around midday (with an air flow rate of 0.02 Kg.s^{-1} , an air layer thickness of 0.03 cm). The figure also shows that the solar cell temperature is highest at around 41.54°C . However, the temperature values of the tedlar and top absorber are almost similar to those of the solar cells ($T_{\text{ted}} = 41.48^\circ\text{C}$ and $T_{\text{absh}} = 41.42^\circ\text{C}$). This means that heat transfer between the PV cells and the absorber plate is taking place, enabling the cooling fluid to lower the cell temperature. The curves obtained conform to the experimental study by TOUAFEK Khaled [9].

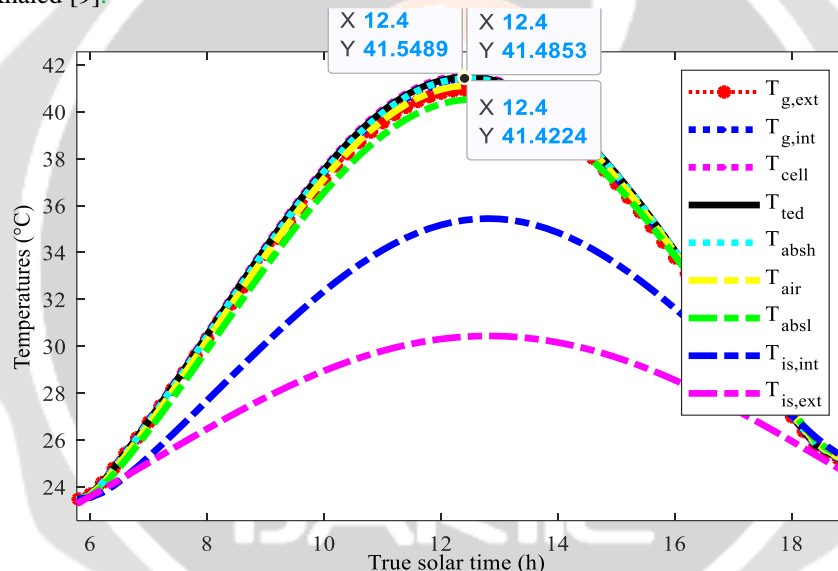


Fig-8 : Temperature trends for each component of the PVT hybrid air collector.

3.5 Hybrid collector electrical power

The figure below shows that the electrical power generated by a photovoltaic solar collector is directly proportional to the solar irradiation received. As irradiation increases, so does current generation, as more photons are available to excite the electrons in the photovoltaic cells. However, the electric current generated can be affected by cell temperature.

The electrical power of a PVT hybrid collector reaches a maximum value of 186.3 W , whereas a conventional PV collector only reaches 163.5 W at around 12 p.m. when solar irradiation reaches its maximum value. Although the system operates under the same weather conditions, the hybrid collector is able to generate more electrical power because it incorporates heat recovery elements. What's more, the addition of fins improves heat transfer between the absorber plates and the cooling fluid by increasing the contact surface with the heat transfer fluid (air). Even though the fins are not in direct contact with the cells, they help improve the rate of heat dissipation from the absorber plate, resulting in an indirect drop in PV cell temperature. The fins also help maintain a constant, even flow of coolant. As a result, cell temperatures are kept lower and more stable.

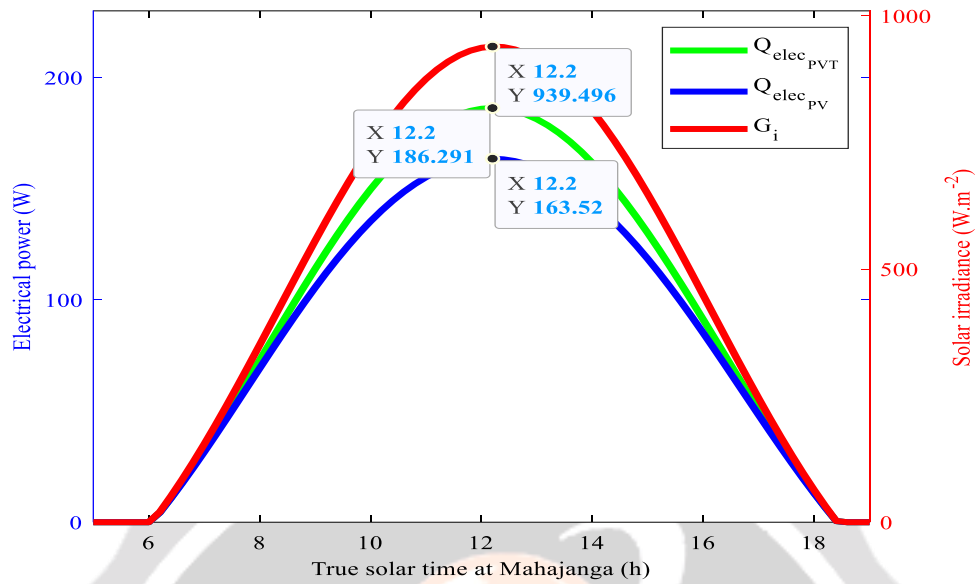


Fig-9 : Variation in electrical power and solar irradiance

3.6 Electrical efficiency

The electrical efficiency of photovoltaic cells increases with decreasing solar cell temperature and increasing solar irradiance. Figure 10 shows that the PVT's electrical efficiency over the course of a day reaches 0.14% at around 12 noon, whereas the conventional PV collector achieves only 0.12% in Mahajanga's climate. The reason for the difference in these yields is the action of a cooling system that immediately reduces the temperature of the PV cells, improving electrical performance. The red curve also shows the variation in overall PVT efficiency, which is the sum of electrical and thermal efficiency. This overall efficiency is relatively stable between 9 a.m. and 4 p.m., as the cooling system keeps the recovered thermal heat in balance and stabilizes the rise in cell temperature.

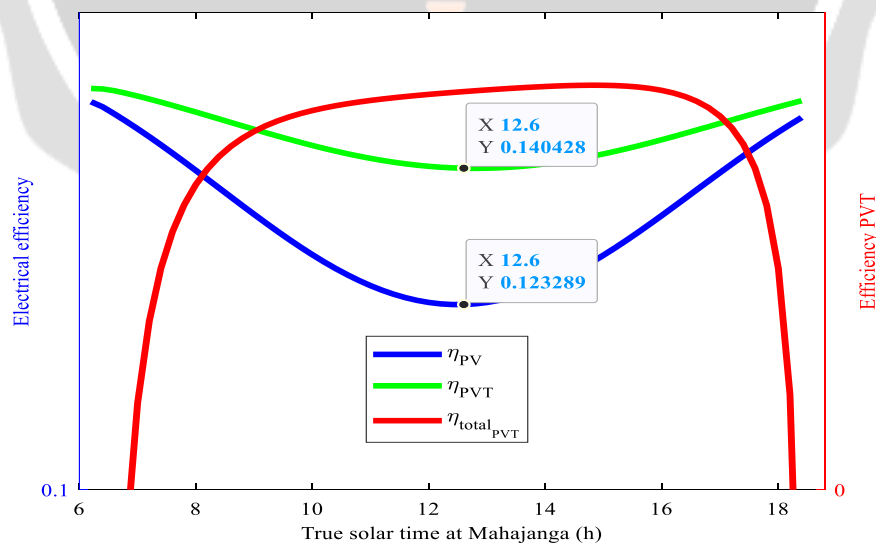


Fig-10 : Electrical efficiency

3.7 PVT-CCP-H system performance

Simulation of the temporal evolution of the electrical power and electrical efficiency of a PVT-CCPH system is carried out by fixing the value of the air mass flow rate and the height of the air duct, and varying the CCP concentration ratio by $C = 1, 1.2, 1.4, 1.6, 1.8, 2, 2.2, 2.5$ (Figure 11). The results obtained show that electrical power changes with increasing concentration level. The higher the concentration level, the greater the maximum power achieved. For concentration ratio $C = 1$, the electrical power value is 186.3 W around midday, while it reaches 430.363 W for $C = 2.5$. For the PVT-CCPH electrical efficiency, the efficiency value increases progressively as the concentration level decreases. For $C = 2.5$, the efficiency is 0.13%, then increases. For $C = 1$, the efficiency is 0.14%.

This performance is due to the presence of the cooling system. Figure 9 also shows that the electrical efficiency of a conventional PV collector without concentration is slightly lower than that of PVT-CCPH for the concentration ratio $C = 2.5$. This shows that the electrical performance of the PVT-CCPH system is efficient.

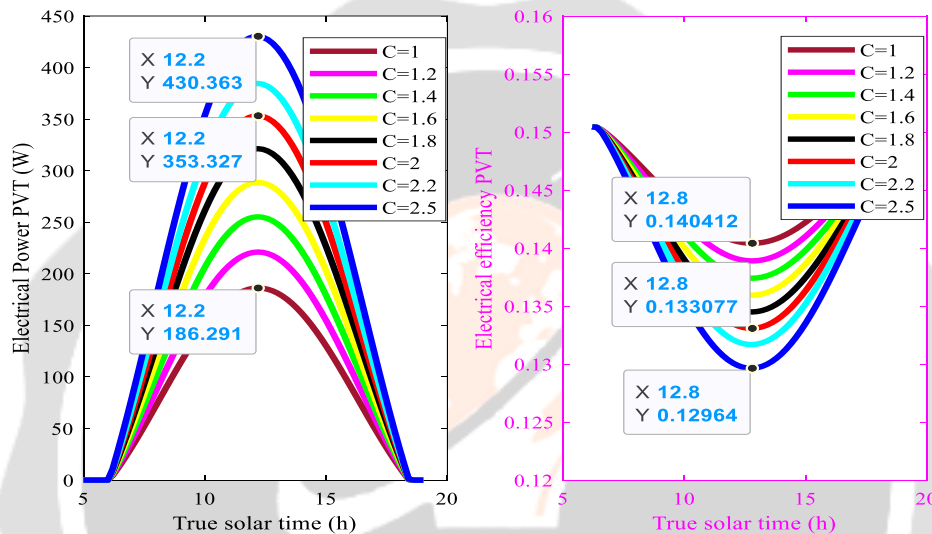


Fig.11 : Variation in electrical power and electrical efficiency of PVT-CCP-H.

Compared with conventional PV and PVT collectors without concentration, the PVT system with concentration (PVT-CCPH) performs better. Figure 12 compares the I-V-P characteristics of PV, PVT and PVT-CCPH air collectors. Adding two CCP and Heliostat reflector systems to a PVT photovoltaic system also offers several advantages. In addition to increasing the concentration acceptance angle product that can be achieved by the system, more uniform irradiation onto the solar cell can also be achieved. These results are in good agreement with the experimental results of Ahed Hameed Jaaz [24].

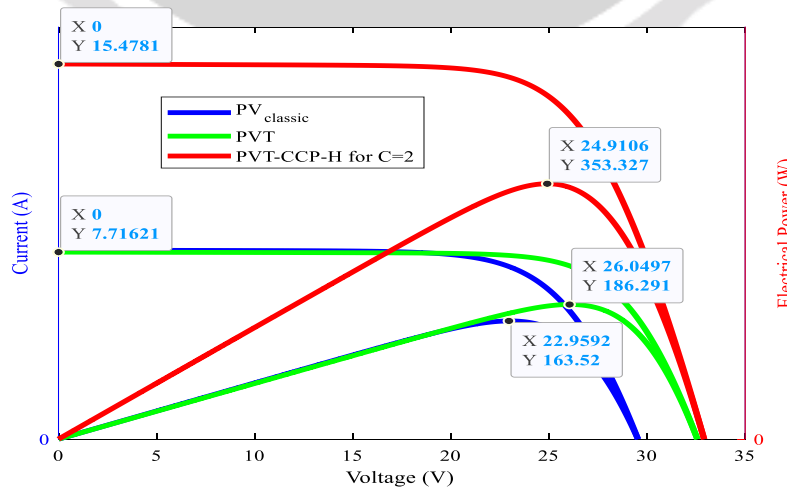


Fig.12 : I-V-P characteristic between PV, PVT and PVT-CCPH modules

3.8 Electrical performance of the MPPT-controlled PVT-CCPH

Figure 13 shows the evolution of current, voltage and electrical power generated by the PVT-CCPH system coupled with an MPPT, a boost converter and a resistive load, as well as the simulation of the dynamic response of a boost converter. For $C = 2$, these results show that the boost converter fulfills its role by increasing the output voltage of the PVT-CCPH to a higher value (110 V) that is suitable for the 35Ω resistive load. On the other hand, the output current is proportionally reduced by around 3 A to maintain the electrical power balance. We can also see that the electrical quantities (current, voltage and power) output vary as a function of time. Initially ($t = 0$ to 0.01 s), the electrical values start at zero, then increase directly. This indicates that the boost output is beginning to be controlled by a control system. This is followed by a gradual increase in electrical values between 0.01 and 0.5 seconds, indicating a transient phase in which the system begins to respond to control. After 0.5 seconds, these values stabilize, meaning that the system reaches its steady state. This shows that the boost converter is operating stably.

In addition, these results show the absence of overshoot or overvoltage, which indicates that the control is well tuned, as the response is quite smooth, without fluctuation or instability, and also without excessive oscillation in the dynamic response. So, choosing the maximum power point tracking algorithm (like P&O) is effective for improving performance in terms of tracking speed and accuracy. The outgoing electrical power reached is 346 W, which is close to that of the incoming power of around 353.3 W, despite losses due to switching, passive elements (inductor, capacitor) and diodes.

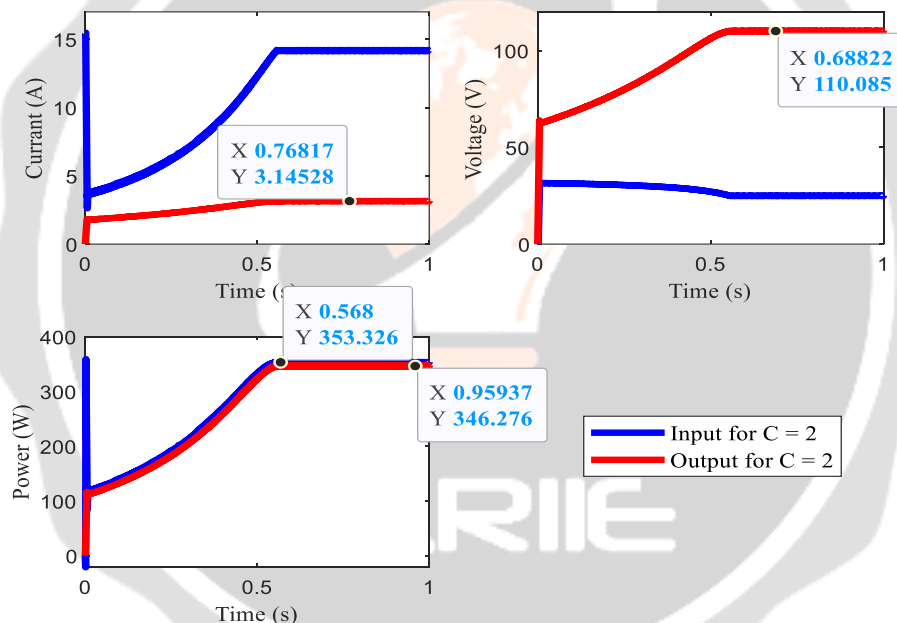


Fig-13 : Temporal evolution of electrical quantities (I-V and P) controlled by MPPT (P&O)

4. CONCLUSION

The aim of this work is twofold : to increase the thermal and electrical efficiency of the collector, i.e. its electrical and thermal output by lowering the operating temperature, and to use this same heat to heat air for product drying. Optimizing the performance of the PVT-air hybrid system involves coupling a Photovoltaic-Thermal air collector, a Cylindro-Parabolic Concentrator, a Heliostat (PVT-CCPH), an MPPT controller (P&O) and a boost converter. PVT-CCPH hybrid collectors are true cogeneration systems, enabling the simultaneous production of electrical and thermal energy. The use of an additional solar concentrator increases the temperature of the hybrid collector, thereby improving its thermal energy yield. The addition of a heat exchanger with fins attached to the absorber further enhances thermal performance, but risks reducing the electrical efficiency of the hybrid collector, which is highly dependent on the collector's operating temperature. Page's model will be used to theoretically determine solar

irradiance. The results of the numerical simulation of the thermal behavior of the photovoltaic-thermal hybrid collector show that the cooling system significantly improves the efficiency of the PV module. With well-defined simulation conditions and iterative calculation, the PVT-CCPH hybrid collector with cooling systems succeeded in lowering the temperature of the PV cells by 41.5°C, giving a significant efficiency of around 0.14% (for $C = 1$), whereas this temperature is around 65°C without the cooling system. The choice of the maximum power point (P&O) tracking algorithm is also relatively effective in improving performance in terms of tracking speed and accuracy. The P&O method succeeded in maintaining and reaching the maximum power point, despite disturbances due to changes in temperature and concentration. The optimized electrical power output of the PVT-CCPH system is 346 W, for $C = 2$. The stable, surge-free electrical power output of the boost indicates a reliable electrical energy performance of this coupling. However, the performance of the PVT-CCPH hybrid system depends on the PVT's external and internal parameters, and above all on effective heat management. Although increased solar irradiation is advantageous for electrical energy production, it must be managed to avoid negative effects such as overheating or reduced cell efficiency. It is therefore logical that the remainder of this work should focus on studying the thermal energy performance of the PVT-CCPH system, as well as the influence of external and internal parameters, in order to find a compromise between these energy performances.

5. REFERENCES

- [1]. DONA Victorien Bruno, 'Modelisation et conversion des irradiations solaires en vue de la production d'énergie renouvelable à Mahajanga', Habilitation to direct research, University of Mahajanga, Madagascar, August 28, 2019.
- [2]. El-YAHYAOUI Sara. 'Photovoltaïque à concentration: optimisation de l'étage secondaire', cotutelle thesis, Université Sidi Mohamed Ben Abdellah & Université de Lorraine, March 26, 2021.
- [3]. Olfa Bel Haj Brahim Kechiche, 'Concentrator Photovoltaic (CPV) : Maximum Power Point Techniques (MPPT) Design and Performance', University of sousse, researchgate, 2021.
- [4]. BOUAMRA M. 'Etude de la distribution du flux au foyer d'une centrale solaire à tour sous sollicitations variables', thesis, University of Blida, February 2020.
- [5]. BELHANI. A. Y and ABRAOUI. O., 'Conception et fabrication d'un heliostat pour une toure solaire', dissertation, Université Kasdi Merbah - Ouargla, 29 Mais 2017.
- [6]. RAHMANI DJELLOUL, 'Analyse d'un système de concentration solaire pour la production d'hydrogène (cas de l'Algerie)', Dissertation, Univeristé Hassiba Benbouali de Chlef, 2012.
- [7]. BELKACEM Mourad, 'Etude et optimisation du transfert d'énergie électrique en conversion photovoltaïque par la recherche du point de puissance maximal (MPPT)', Dissertation, Université Abou Belkaid de Tlemcen, 2015.
- [8]. TABET Ismail. 'Etude, Réalisation et simulation d'un capteur solaire', thesis, Université des freres mentouri constantine, 2016.
- [9]. TOUAFEK Khaled, Contribution à l'étude et à la conception d'un système énergétique utilisant des capteurs hybrides photovoltaïques thermiques, thesis, Ecole Normale Polytechnique ENP, Algeria, 2010.
- [10]. S. Ben Mabrouk, 'Etude et Simulation d'un Capteur hybride Photovoltaïque Thermique à air', University of Tunis El Manar, Researchgate, 2016.
- [11]. Oussama El Manssouri, B. Hajji, Giuseppe M.T, Antonio G. and Stefano A., 'Electrical and Thermal Performances of Bi-Fluid PV/Thermal Collectors'. *Energies* 2021, 14, 1633.
- [12]. Kamel Shalaoui, Hatem Oueslati & Salah Ben Mabrouk, 'Thermal and electrical performance evaluation of hybrid air PV/T collector - numerical analysis and experimental study', *International journal of Sustainable Energy*, 2021.
- [13]. HAYIBO. K. S, 'Modelisation et simulation d'un capteur solaire hybride photovoltaïque thermique', Dissertation, Université Ouaga, 2016.
- [14]. Khelifa Abdelkrim, 'Contribution à la conception et modelisation d'un capteur solaire hybride photovoltaïque thermique PVT', Thesis, Universtité Hadj Lakhdar de Batna, 2017.
- [15]. MEKADEM Hafsa and Mellouki H, 'Etude paramétrique d'un capteur hybride doté d'un concentateur parabolique composé (PVT-CPC)', Dissertation, Université Ahmed Draia-Adrar, 2022.
- [16]. Incropera, F.P.; DeWitt, D.P. *Fundamentals of Heat and Mass Transfer*, 6th ed; John Wiley & Sons, Inc: Hoboken, NJ, USA, 2007.
- [17]. GHELLAB Amel, 'Modelisation et optimisation des capteurs solaires hybrides', thesis, Université des frères Mentours Constantine, 2018

- [18]. A. Ghellab, A. Kaabi et al, 'Les retombées technico-économique d'un capteur hybride photovoltaïque/thermique à air', Revue des Energies Renouvelable Vol. 16 N°3 (2012) 425-550.
- [19]. BOUHOREIRA Y. and GANA L. 'Etude de l'effet des paramètres sur les performances d'un collecteur solaire cylindro parabolique', dissertation, Université Kasdi Merbah Ouargla, 24-06-2018.
- [20]. C. El Fouas, O. El Manssouri, B. Hajji et al, 'Study and Modeling of Energy Performace of PV/T Solar Plant for Hydrogen Production', Engineering and Renewable Energy Systems, 2021.
- [21]. Amina Benhammou. "Optimisation d'un nouveau système de séchage solaire modulaire pour plantes aromatiques et médicinales," thesis, University Abou Bekr Belkaid, Algeria, Feb. 2010.
- [22]. DONA Victorien Bruno, MAXWELL Djaffard, et al, "Estimate of photovoltaic energy production during the sunniest month in Mahajanga", IJARIE-ISSN(O)-2395-4396, Vol-5 Issue-4, pp. 92 - 103, 2019.
- [23]. HARITHI BEN Daoud Ben Attoumane, PASERA Joanès Keneddy and DONA Victorien Bruno, 'Energy performance studies of a PVT-air hybrid system with caes: influence of input parameters on the compression system', IJARIE-ISSN(O)-2395-4396, Vol-10 Issue-4 2024
- [24]. Ahed Hameed Jaaz, Husam A. H, Kamaruzzaman S., Abdul Amir H. K., Tayser Sumer G. and Ahmed A. Al-Amiery , 'Outdoor Performance Analysis of a Photovoltaic Thermal (PVT) Collector with jet Impingement and Compound Parabolic Concentrator (CPC), Materials 2017, 10, 888.

